Revealing the Underlying Patterns: Investigating Dataset Similarity, Performance, and Generalization

Akshit Achara^a, Ram Krishna Pandey^a

^aGE Research, Bangalore, India

ARTICLE INFO

Keywords: Segmentation Generalization Explainability Similarity Computer Vision

ABSTRACT

Supervised deep learning models require significant amount of labelled data to achieve an acceptable performance on a specific task. However, when tested on unseen data, the models may not perform well. Therefore, the models need to be trained with additional and varying labelled data to improve the generalization. In this work, our goal is to understand the models, their performance and generalization. We establish image-image, dataset-dataset, and image-dataset distances to gain insights into the model's behavior. Our proposed distance metric when combined with model performance can help in selecting an appropriate model/architecture from a pool of candidate architectures. We have shown that the generalization of these models can be improved by only adding a small number of unseen images (say 1, 3 or 7) into the training set. Our proposed approach reduces training and annotation costs while providing an estimate of model performance on unseen data in dynamic environments.

1. Introduction and Related Work

Deep Learning tasks like segmentation are commonly performed by using supervised techniques. This requires labelled data for consumption by the model. If the model is not trained on diverse data, it can overfit and may not perform well on unseen data. It might also be the case that the model is not expressive enough to handle the variations in the training data thereby showing poor performance. So, the model needs to be trained with additional data points from unseen data to achieve better performance. This boils down to the question: "how much additional labelled data is required?".

Therefore, an analysis of model performance and behaviour on test and unseen data is required. Generally, test datasets have similar distribution to the training datasets but unseen datasets may or may not have similar distribution. Hence, it requires us to obtain a metric that can tell how far these unseen datasets are from the training dataset. In order to accomplish this task, we need to compare datasets by systematically evaluating the images in one dataset against all images in the other dataset. Comparison of the raw images is computationally expensive and is not robust to the variations such as lightning, illumination, orientation, etc. Therefore, we extract feature vectors as the representative of images.

Classical approaches utilizing structural similarity [1] and histogram of oriented gradients [2] have been used to find descriptors and keypoints from the images. These methods have been commonly used to distinguish noisy images from a set of images.

Deep learning techniques based on Siamese networks [3] have been commonly used for computing image similarity. In [4], the authors use labelled matching and non-matching pairs of images and use CNNs to get feature vectors which are used in a siamese architecture using contrastive loss. It is

f2016953p@alumni.bits-pilani.ac.in (A. Achara); ramp@alum.iisc.ac.in (R.K. Pandey)

not suitable for our task as it focuses on a classification task that requires labelled pairs of matching and non matching images.

While the above methods are focusing towards image similarity, in [5], the authors proposed an optimal transport solution to compute the distance between the datasets. However, the notion of a dataset includes the labels and images which is not suitable for our goals as we want to allow the analysis of unseen datasets.

These approaches consider the distance between images and between the datasets in a general scenario. Distances can have different meaning for different models depending on their architecture and training.

In [6], the authors analyzed how well a deep metric learning model is able to perform on unseen data. The work is focused on image similarity and matching.

In [7], the authors propose an open world image segmentation framework to detect whether the objects are in or out of distribution(OOD). The framework also includes a module to adapt to the OOD objects using few-shot learning.

In [8], the authors propose techniques to comprehend generalization capabilities of UNets for classification and regression tasks without requiring ground truth annotations and in [9], the authors develop a notion of similarity on training and unseen data; and study how the performance is correlated with the similarity metrics in consideration.

In [10], the authors show that addition of more training examples may not always improve the model performance and a better data selection strategy can help.

In [11], the authors have visualized the neural network generalization from an optimization and loss perspective.

In this work, we have explored the relationship between the distances (image-image, image-dataset and dataset-dataset), performance and generalization of deep learning models. We have selected publicly available datasets (see section 2 for more details) for our experiments and analysis.

Research in this direction can have significant contributions in the applications that necessitate the selection of

diverse datasets to train models capable of generalizing to new datasets. It is also relevant in scenarios like domain adaptation.

1.1. Contributions

Our main contributions are as follows:

- a) We proposed a distance metric to obtain the distances between datasets (O^{dist}) and between images and datasets (I^{dist}) that can be related to the performance of the model.
- b) If the F-score is consistent (F-score vs I^{dist} curve is a line parallel to the x-axis) across all the unseen images (see figure 4), model need not be finetuned saving energy and labelling cost.
- c) We have shown that selecting a few images from an unseen dataset, can significantly boost its performance thereby improving the generalization and reducing annotation cost (see figures 5, 6, 8 and 9).
- d) Our study can give a relative comparison of models and their tradeoffs that can possibly help in selecting the most suitable model based on the requirements (see section 6 for more details).
- e) We have found that models like segment anything [12] and adapted segment anything [13] require additional data to perform well across multiple unseen datasets for a specific task (see section 11 in appendix and figure 9 for details).

2. Datasets

2.1. Crack Datasets

- a) CrackTree260 (P): It contains 260 road pavement images.
- b) CrackLS315 (S_1): It contains 315 road pavement images of size 512 \times 512.
- c) CRKWH100 (S₂): It contains 100 road pavement images of size 512 × 512.
- d) **GAPS** (S_3): It contains 509 images of size 448 × 448 selected from the kaggle crack segmentation dataset.
- e) **FOREST** (S_4): It contains 118 images of size 448×448 selected from kaggle crack segmentation dataset.

2.2. Non-Crack Datasets

- a) **PASCAL-VOC** (S_5): It is a dataset [14] with 20 classes and multiple tasks like Classification, Detection, Segmentation and Action Classification (10 classes) are defined on it. We randomly selected 500 images from the dataset to create a fixed new dataset (S_5) for all the experiments in this study.
- b) **BSDS500** (S_6): It is a dataset [15] that contains 500 images of size 421×321 commonly used for benchmarking on segmentation and boundary detection tasks.
- P, S_1 and S_2 were obtained from [16] and, S_3 [17] and S_4 were obtained from [18]. In this work, the dataset P is considered as the primary dataset and the datasets S_i , $i \in \{1, 2, 3, 4, 5, 6\}$ will be referred as the secondary datasets (S will be interchangably used with S_i). We resized all the images to 448×448 for all the experiments.

Model	Feature Vector
SAM	The image embeddings from the image encoder (MAE pre-trained Vision Transformer (ViT)[24]) of the SAM[12].
CLIPSeg	The concatenated hidden states' outputs from the CLIP decoder [19] with the input text prompt "line structures".
ENet	The last layer(before the classification head) of a pretrained Efficient-Net [20] Model on imagenet.
DC	The concatenation of all the down-sampling layers' outputs of the encoder as shown in the architecture of DC[16].
UNet ⁺⁺	The concatenation of all the skip connections from the EfficientNet encoder [20] used as backbone in <i>UNet</i> ⁺⁺ .
ADSAM	The image embeddings from the image encoder discussed in [13].

Table 1

The table shows the model and the details of the corresponding feature vector extracted from it. The details of the models can be seen in section 3.1.

3. Methodolgy

3.1. Image Representation

We considered multiple models to get feature vectors from the images, namely Segment Anything Model [12] ("base" version is used in this study), CLIPSeg [19] (segmentation model to perform image segmentation using text and image prompts), EfficientNet [20] model pretrained on imagenet [21] dataset, DeepCrack [1] which is a specialized model for crack segmentation (hereafter referred as DC), UNet++ [22] initialized with an EfficientNet backbone (hereafter referred as UNet++) and an adapted version of SAM that can be trained on custom datasets [13] (hereafter referred as ADSAM).

In [23], the authors propose a contrastive languageimage pre-training (CLIP) model to find the most relevant text given an image. In this work, we use the modified CLIP (CLIPSeg [19]) model where a decoder is added to perform segmentation tasks. We obtain the feature vectors by concatenating the outputs of all hidden layers of the decoder by giving input text prompts along with the images to the CLIPSeg model. The checkpoint used can be seen here¹.

We extract the feature vectors from each model to obtain a meaningful high dimensional feature representation of images.

3.2. Distance Computation

The high dimensional feature vectors obtained from the models are projected into a low dimensional representation

 $^{^{1}}$ https://huggingface.co/CIDAS/clipseg-rd64-refined

using PCA to capture the distinguishing features while reducing the complexity of comparing multiple images and datasets.

We considered feature vectors extracted from all images of two datasets at a time for projection (into a low dimensional space) where one dataset set is always P and the other is one of the secondary datasets S. We use 25 principal components together for the study as we observe stability in distance computation (see section A.1 in appendix for more details).

We compute the pairwise distances between the images of P and S using the low dimensional vectors to obtain a distance matrix as shown in equation 6. Sum of each row of the pairwise distance matrix represents image-dataset distance(I^{dist}) i.e. the distance of each image in S from all of P, and mean of all the rows taken together represent dataset-dataset distance(O^{dist}) i.e the overall distance of S from P. See equation set 7 for more details. The O^{dist} can be computed for dataset of different sizes since it is equal to the mean I^{dist} .

Since the proposed distance metrics are only utilizing images and not labels, the distance computation can be used for multiple other tasks like classification, object detection and even for the other data types. However, the feature vectors should be extracted based on the input and model architecture such that the input features are captured. The entire computation process can be seen in the figure ??.

$$F(x) = y; x \in R^{h \times w}, y \in R^q \tag{1}$$

Equation set 1: The feature extractor (F) maps the input image to a feature vector. Here, $h \times w$ represents the size of the input image i.e. 448×448 .

Equation set 2: P_H and S_H represent the feature vectors of primary and secondary datasets respectively where each q-dimensional row represents a feature vector of an image. Here, n is the number of images in the primary dataset and m is the number of images in the secondary dataset.

$$X = \left\{ P_H^{\mathsf{T}} \middle| S_H^{\mathsf{T}} \right\}_{(n+m)\times q}^{\mathsf{T}}$$

$$X = \left\{ \begin{array}{c} X_1 \\ X_2 \\ \vdots \\ X_{(n+m)} \end{array} \right\}_{(n+m)\times q}$$

$$\bar{X} = \frac{1}{(n+m)} \sum_{j=0}^{(n+m)} X_j$$

$$A = X - \bar{X}$$

$$(3)$$

Equation set 3: A in the centered input for the PCA.

$$A = \bigcup_{(n+m)\times(m+n)} \sum_{(n+m)\times q} V^{\top}$$

$$A^{\top}A = V \sum_{n=0}^{\top} U^{\top}U \sum_{n=0}^{\top} V^{\top}$$

$$= V \sum_{n=0}^{\top} \sum_{n=0}^{\top} V^{\top}$$

$$= V D V^{\top}$$
(4)

Equation set 4: Here, U and V are orthogonal matrices i.e. $U^{T}U = V^{T}V = I$. V represents the eigen vectors and D represents the eigenvalues.

$$V_{(n+m)} = \begin{cases} v_{11} & v_{12} & \dots & v_{1q} \\ v_{21} & v_{22} & \dots & v_{2q} \\ v_{31} & v_{32} & \dots & v_{3q} \\ \vdots & \vdots & \dots & \vdots \\ \vdots & \vdots & \dots & \vdots \\ v_{1q} & v_{2q} & \dots & v_{qq} \end{cases}$$

$$V_{z} = \begin{cases} v_{11} & v_{12} & \dots & v_{1z} \\ v_{21} & v_{22} & \dots & v_{2z} \\ v_{31} & v_{32} & \dots & v_{3z} \\ \vdots & \vdots & \dots & \vdots \\ \vdots & \vdots & \dots & \vdots \\ v_{q1} & v_{q2} & \dots & v_{qz} \end{cases}$$

$$Y_{q1} = AV_{z}$$

$$Y = \begin{cases} P_{L}^{\mathsf{T}} | S_{L}^{\mathsf{T}} \rangle_{(n+m)\times z}^{\mathsf{T}} \end{cases}$$

$$(5)$$

Equation set 5: Y consists of a low dimensional representation of the feature vectors of P and S obtained using PCA (implementation taken from here [25]).

$$D(S, P) = \begin{cases} d(s_1, p_1) & d(s_1, p_2) & \dots & d(s_1, p_n) \\ d(s_2, p_1) & d(s_2, p_2) & \dots & d(s_2, p_n) \\ d(s_3, p_1) & d(s_3, p_2) & \dots & d(s_3, p_n) \\ \vdots & \vdots & \dots & \vdots \\ d(s_m, p_1) & d(s_m, p_2) & \dots & d(s_m, p_n) \end{cases}$$

$$d(a, b) = \|a - b\|_2$$
(6)

Equation set 6: D(S, P) refers to the pairwise distance matrix where each value in the matrix is the euclidean distance between each image of S and P. s_j represents the low dimensional feature vector from S_L and p_k represents the low dimensional feature vector from P_L . Here, $j \in \{1, 2, ..., m\}$ and $k \in \{1, 2, ..., n\}$. From here onwards, we can consider S_L and P_L are represented by S and P in the context of distance computation.

$$I^{dist}(S, P) = \begin{cases} \sum_{j=1}^{n} d(s_{1}, p_{j}) \\ \sum_{j=1}^{n} d(s_{2}, p_{j}) \\ \sum_{j=1}^{n} d(s_{3}, p_{j}) \\ \vdots \\ \sum_{j=1}^{n} d(s_{m}, p_{j}) \end{cases}$$

$$I^{dist}(S, P) = \begin{cases} I_{1}^{dist}(S, P) \\ I_{2}^{dist}(S, P) \\ \vdots \\ I_{m}^{dist}(S, P) \end{cases}$$

$$O^{dist}(S, P) = \frac{1}{m} \times \sum_{j=1}^{m} I_{j}(S, P)$$

Equation set 7: I^{dist} represents the distance of each image in S from P and O^{dist} represents the distance between S and P.

3.3. Performance Computation

We use F-score and perceptual quality (to resolve a few overlap boundary cases when we felt that the F-score is not discriminative) as the two main parameters to evaluate a model's performance. The F-score of crack pixels computed by choosing a threshold that results in the highest F-score over all the images considered for evaluation; has been used as the performance metric. It is also known as Overall Dataset Score (ODS) and the computation is adapted from here². It is to be noted that the performance metric

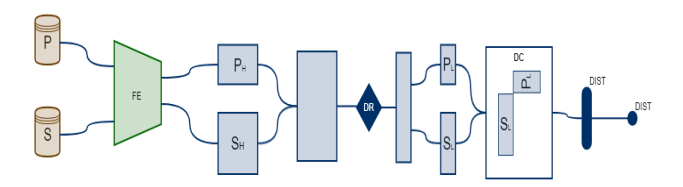


Figure 1: The figure shows the distance computation process discussed in the section 3.2. FE is the feature extractor/model from which high dimensional feature vectors P_H and S_H are obtained. The DR (dimensionality reduction) using PCA results in low dimensional representations P_L and S_L . Finally, the I^{dist} and O^{dist} are computed using the paiwise distance matrix shown in the DC(distance computation) block.

(ODS) is chosen with respect to the task in consideration i.e. segmentation and a suitable performance metric can be chosen based on the required tasks like classification, object detection, etc.

4. Experiments

4.1. Crack vs Non Crack Distinguishability

There is a significant difference in the visual representation of the crack and non-crack datasets, our goal is to show that the differences are captured by the selected pretrained models (namely SAM, CLIPSeg and ENet). To quantify these differences, we compute the $O^{dist}(S, P)$ (as discussed in section 3.2) of each of the secondary datasets S from the primary dataset P using these models.

These pretrained models can capture the global contexts as they are trained on large datasets having different backgrounds. This suggests that we can use the distance metric to distinguish different datasets. However, these pretrained models are not trained to perform crack segmentation (for more details, see section B.1 and B.2). Therefore, to understand the relationship the distances among the crack datasets, we selected three architectures namely DC, UNet⁺⁺ and ADSAM to train on P and computed the distances of the secondary crack datasets from P along with the performance on these secondary datasets.

DC is trained using scripts provided here³, UNet⁺⁺ is initialized with an EfficientNet-B3 backbone[20] and trained with a multi-gpu setup using segmentation models pytorch[26] and pytorch lightning[27] and ADSAM is trained using the "base" version of SAM[12]. The training scripts for ADSAM can be found here⁴.

4.2. Distance and Performance

The distinguishability of images within each crack dataset for DC, UNet⁺⁺ and ADSAM is analyzed. The performance of these models is computed on the secondary crack datasets $S(S_1, S_2, S_3)$ and S_4 . Within the same dataset, a set of

 $^{^2 \}verb|https://github.com/yhlleo/DeepSegmentor/blob/master/eval/prf_metrics.py|$

³https://github.com/qinnzou/DeepCrack

 $^{^{4} \}verb|https://github.com/chenyangzhu1/SAM-Adapter-PyTorch|$

images can be closer to P whereas another set of images can be farther from P. It is expected that the model performance will be better on the images closer to P as compared to those that are farther. To validate the same, we perform the following analysis.

4.2.1. Intra Dataset Analysis

Firstly, we compute the $I^{dist}(S,P)$. The images are then sorted in ascending order of distances $I^{dist}(S,P)$ and divided into two equal parts based on the distance. The F-score (F_1,F_2) , mean distances (μ_1,μ_2) and standard deviations (σ_1,σ_2) of each part are computed. The same computation is repeated by splitting the dataset into 3 equal parts to show the difference in performance between the closest and farthest images of S from P. A plot 10 of sorted images vs distance from P can be seen in the appendix.

$$\mu_{1} = \frac{1}{\frac{m}{2}} \sum_{j=1}^{\frac{m}{2}} I_{j}^{dist}(S, P)$$

$$\mu_{2} = \frac{1}{\frac{m}{2}} \sum_{j=\frac{m}{2}+1}^{m} I_{j}^{dist}(S, P)$$

$$\sigma_{1} = \frac{1}{m/2} \sum_{j=1}^{m/2} I_{j}^{dist}(S, P) - \mu_{1}$$

$$\sigma_{2} = \frac{1}{\frac{m}{2}} \sum_{j=\frac{m}{2}+1}^{m} I_{j}^{dist}(S, P) - \mu_{2}$$
(8)

Equation set 8: (μ_1, μ_2) and (σ_1, σ_2) are the means of the first half and second half of the sorted $I^{dist}(S, P)$. Computation can be performed for three parts similarly.

4.3. Model Adaptation

We perform an experiment by randomly selecting n (from P)+q (from S) images (n = |P| and $q \in \{1,3,7\}$) from the images of each dataset S based on $I^{dist}(S,P)$ to train the models i.e addition of 1,3 and 7 images from each S into the training dataset to obtain three models with different adaptations. The next step is to compute the $I^{dist}(S,P)$ and F-score on S. The F-score vs $I^{dist}(S,P)$ plots of the adapted models are compared with the models trained on P. For plotting, we perform a moving average with a window size of |S|/10 on the F-scores and a min-max scaling on $I^{dist}(S,P)$. In min-max scaling, we scale a set of numbers x into a range of 0-1 by using the absolute minimum and maximum values of x and get $x_{scaled} = (x - x_{min})/(x_{max} - x_{min})$. The images were selected at a distance of 0.6-1 after the min-max scaling.

4.4. Model Understanding

To understand the behaviour of the models on images different from the crack images, we perform inference using the models (DC, UNet⁺⁺ and ADSAM trained on P) on the images from the BSDS500[15] dataset. The motivation

is to observe the masks produced by these models and understand whether the model is actually predicting cracks or is predicting crack like features/edges from the images. If a model extracts crack like features from every image as cracks, it may give ambiguous distances.

5. Results

The table 2 and figure 3 shows the distances computed from all the selected models (see details of the models in table 1). The non-crack datasets S_5 and S_6 are the farthest from P for all the models except for DC where the model's focus is on the edges present in the images (see figure 2).

Since there is a tradeoff between the precision and recall, we can decide the kind of model required for the task in hand. The figure 2 gives a good understanding on the behaviour of the models. In figure 2, the deepcrack model is more confident in detecting edge like structures compared to ADSAM and UNet⁺⁺. This suggests that ADSAM can be used for high precision and DC for high recall.

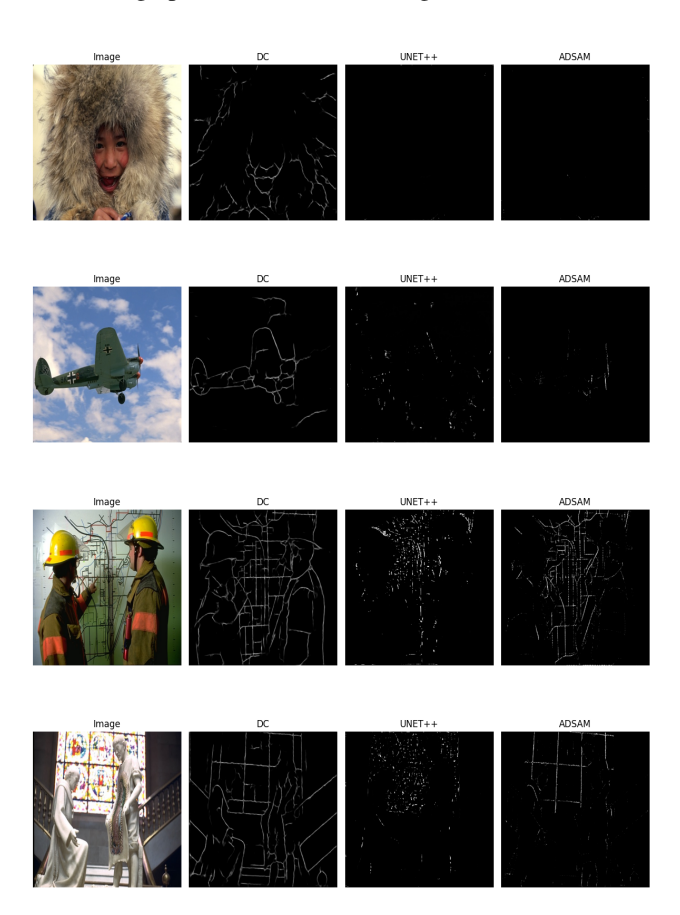


Figure 2: Shows (a) original image, (b) DC , (c) UNet⁺⁺ and (d) ADSAM outputs on the images from S_6 . DC model focuses on specific features like edges.

The tables 3 for UNet⁺⁺, 4 for DC and 5 for ADSAM show the F-score and mean distance obtained by the models on each part of each secondary crack dataset (see captions of the tables for more details). The tables 3a and 3b show

	S_1	S_2	S_3	S_4	S_5	S_6
SAM	0.149	0.145	0.164	0.134	0.213	0.195
CLIPSeg	0.135	0.134	0.142	0.153	0.236	0.199
ENet	0.153	0.153	0.159	0.163	0.188	0.183
DC	0.153	0.188	0.153	0.174	0.166	0.167
UNet ⁺⁺	0.056	0.069	0.063	0.054	0.465	0.293
ADSAM	0.166	0.152	0.163	0.148	0.193	0.178

Table 2

The table shows the scaled $O^{dist}(S,P)$. The numbers in each cell are obtained after dividing the $O^{dist}(S,P)$ by the sum of the corresponding row. The top 2 farthest distances for each model from P are shown in bold.

that the performance is also similar for the first and second half on S_1 , S_2 and S_3 but the performance first half is significantly higher than the second half for S_4 . Overall, there is a decreasing trend with distances for the UNet⁺⁺ model. Similarly, the other two models also follow a decreasing trend in the performance with the distances which can be seen in the tables 4a, 4b, 5a and 5b.

The figures 4, 5 and 6 show the F-score vs $I^{dist}(S, P)$ comparison for the models UNet⁺⁺, DC and ADSAM respectively. These plots show the model performance when trained on P, P+1 image from each secondary, P+3 images from each secondary and P+7 images from each secondary dataset. These 1,3 and 7 images from each secondary crack dataset are selected from the last 20% of the images where the performance of the models are significantly lesser in most cases. After the training of the models, we can see a significant improvement in the performance across datasets and images, thereby increasing the generalization of the models (see captions and figure 7 for additional details).

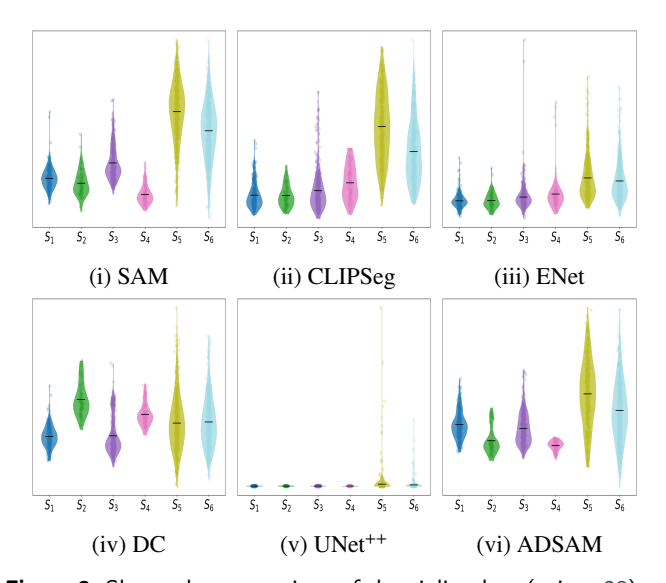


Figure 3: Shows the comparison of the violin plots (using 28) of I^{dist} distribution of all the secondary datasets S from P. The corresponding quantitative results can be seen in 2.

Dataset	$F(\mu,\sigma)[0-50\%]$	$F(\mu,\sigma)[50-100\%]$
S_1	0.483(0.2, 0.06)	0.444(0.54, 0.18)
S_2	0.567(0.24, 0.15)	0.606(0.79, 0.13)
S_3	0.353(0.19, 0.06)	0.316(0.48, 0.16)
S_4	0.241(0.03, 0.02)	0.061(0.4, 0.23)

(a) The table shows the comparison of the performance of first 50% and last 50% images.

Dataset	$F(\mu,\sigma)[0-33\%]$	$F(\mu,\sigma)[67-100\%]$
S_1	0.488(0.18, 0.05)	0.415(0.64, 0.13)
S_2	0.584(0.15, 0.09)	0.622(0.85, 0.1)
S_3	0.365(0.16, 0.04)	0.314(0.56, 0.13)
S_4	0.283(0.02, 0.01)	0.021(0.5, 0.17)

(b) The table shows the comparison of the performance of first 33% and last 33% images.

Table 3

The performance is computed using $UNet^{++}$ trained on P. Each cell in the tables represents the F-score(mean, standard deviation). See details in the section 4.2.1.

Dataset	$F(\mu,\sigma)[0-50\%]$	$F(\mu,\sigma)[50-100\%]$
S_1	0.346(0.21, 0.08)	0.318(0.42, 0.09)
S_2	0.432(0.25, 0.09)	0.464(0.62, 0.19)
S_3	0.461(0.16, 0.04)	0.391(0.42, 0.16)
S_4	0.625(0.24, 0.09)	0.58(0.56, 0.18)

(a) The table shows the comparison of the performance of first 50% and last 50% images.

Dataset	$F(\mu,\sigma)[0-33\%]$	$F(\mu,\sigma)[67-100\%]$
S_1	0.34(0.17, 0.07)	0.30(0.47, 0.1)
S_2	0.43(0.2, 0.08)	0.489(0.7, 0.16)
S_3	0.472(0.14, 0.04)	0.37(0.5, 0.14)
S_4	0.638(0.19, 0.07)	0.58(0.63, 0.17)

(b) The table shows the comparison of the performance of first 33% and last 33% images.

Table 4

The performance is computed using DC trained on *P*. Each cell in the tables represents the F-score(mean, standard deviation). See details in the section 4.2.1.

6. Observations

The results in the figures 4, 5 and 6 show that the performance of models trained on P decreases as the distance increases. This gives a motivation to select a few images ($\{1,3,7\}$) from each of the secondary crack datasets and train the models by adding the selected images into the training data. The trained model seems to generalize on all secondary datasets which can be seen in the figures 4, 5 and 6. Fewer number of images are selected to reduce the labelling cost that can also improve the generalization of the models on different unseen datasets [29].

Overall, the distances are inversely proportional to the performance of the models. However, there are additional factors that can determine the performance of a model on the

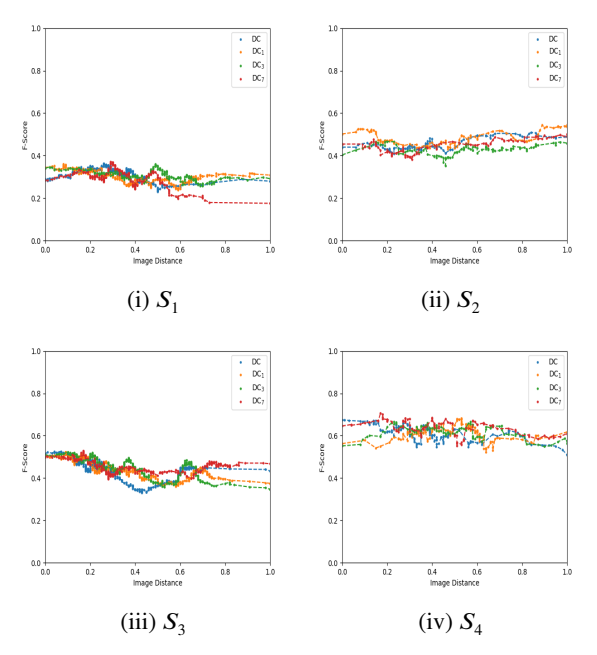


Figure 4: The figure shows the F-score vs $I^{dist}(S,P)$ plot for S. The results are computed using the DC model which was trained on $P+n,n\in\{0,1,3,7\}$ where n images are selected from each S.

Dataset	$F(\mu,\sigma)[0-50\%]$	$F(\mu, \sigma)[50 - 100\%]$
S_1	0.388(0.23, 0.09)	0.4(0.51, 0.14)
S_2	0.392(0.2, 0.08)	0.375(0.56, 0.24)
S_3	0.249(0.19, 0.07)	0.292(0.47, 0.14)
S_4	0.471(0.44, 0.17)	0.33(0.79, 0.1)

(a) The table shows the comparison of the performance of first 50% and last 50% images.

Dataset	$F(\mu,\sigma)[0-33\%]$	$F(\mu,\sigma)[67-100\%]$
S_1	0.383(0.184, 0.07)	0.405(0.584, 0.13)
S_2	0.37(0.16, 0.07)	0.29(0.654, 0.21)
S_3	0.226(0.153, 0.05)	0.293(0.533, 0.12)
S_4	0.462(0.353, 0.15)	0.291(0.842, 0.07)

(b) The table shows the comparison of the performance of first 33% and last 33% images.

Table 5

The performance is computed using ADSAM trained on P. Each cell in the tables represents the F-score(mean, standard deviation). See details in the section 4.2.1.

unseen images. The F-score may not always be an accurate estimate of the performance and the ambiguity in some cases can be resolved using a different metric such as perceptual quality.

If the performance plot vs distance is a near horizontol line parallel to the x-axis, that indicates that the model is consistently performing well across the images (generalizes well) which can help in model selection by observing the plots. In this case, the model has already reached a satisfactory performance and adding new images from \mathcal{S} into the

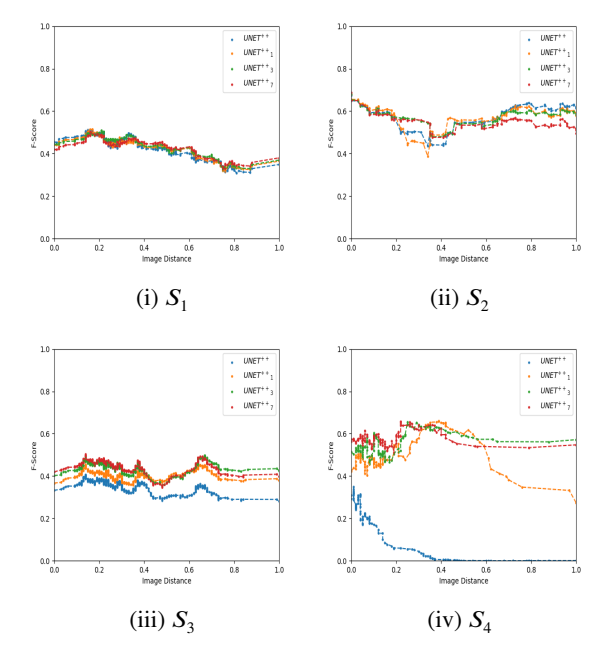


Figure 5: This figure shows the F-score vs $I^{dist}(S,P)$ plot for S. The results are computed using UNet⁺⁺ model which was trained on $P+n,n\in\{0,1,3,7\}$ where n images are selected from each S.

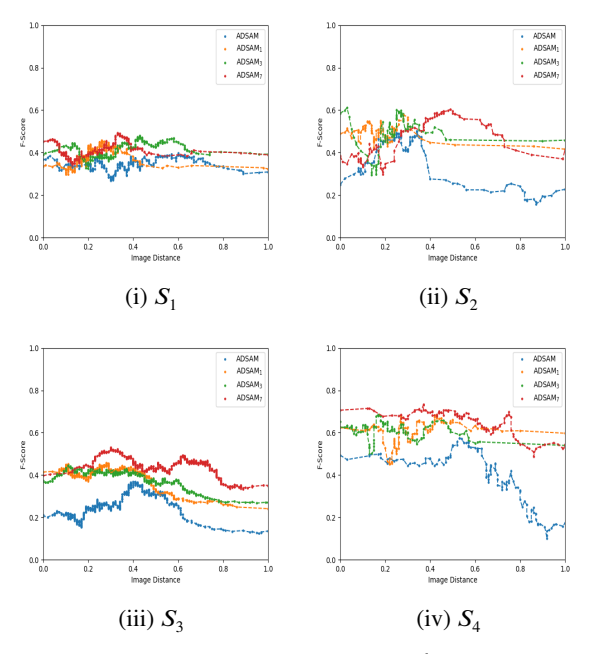


Figure 6: This figure shows the F-score vs $I^{dist}(S,P)$ plot for S. The results are computed using the ADSAM model which was trained on $P+n,n\in\{0,1,3,7\}$ where n images are selected from each S.

training set might not have a significant effect on the generalization of the model. However, the baseline performance can be improved using additional set of images.

The figures 8 and 9 show the qualitative improvement in performance of the models on the dataset where the base

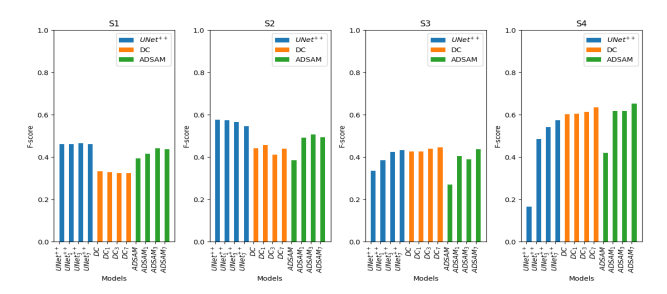


Figure 7: The figure shows the performance (F-score) of each of the models (trained on P) on the secondary datasets, S.

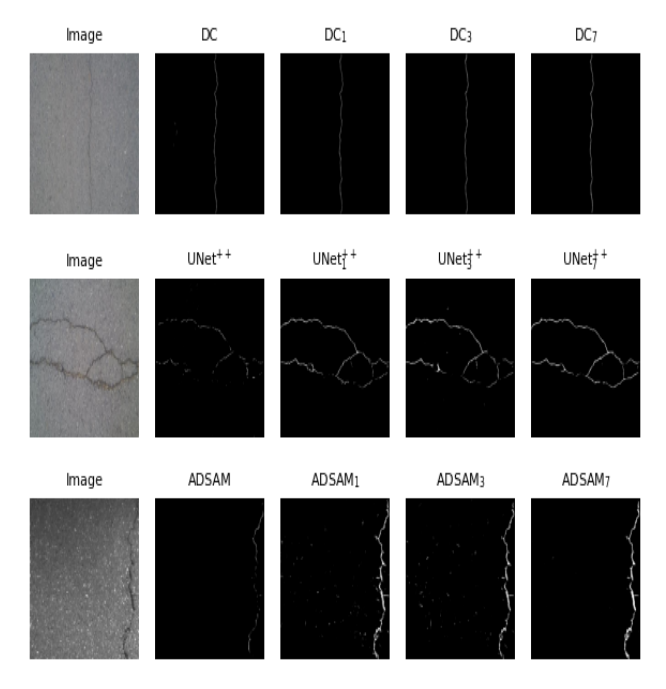


Figure 8: Shows original image, Model, Model₁, Model₃ and Model₇ outputs on dataset. The input image for DC and UNet⁺⁺ is from S_4 and from S_3 for ADSAM. The titles of each figure (except the crack images from the dataset) show the name of model used for inference.

models i.e the models only trained on P are not performining consistently well across all the images from on secondary datasets (see figures 4, 5 and 6 for performance details). In figure 8, the first column shows the input image, followed by the outputs of the models trained on P and the adapted models with 1,3 and 7 images respectively. Figure 9 shows the improvement on a completely blind dataset for all the models. Overall, this suggests that the model is generalizing better across multiple datasets as compared to the base models (where the F-score vs I_{dist} curve is near parallel to the x-axis, see figuress 4, 5 and 6).

7. Conclusion

Our study analyzes multiple datasets to demonstrate that the performance of the models can be related to the proposed distance metrics (see figures 4, 5 and 6). This helps in

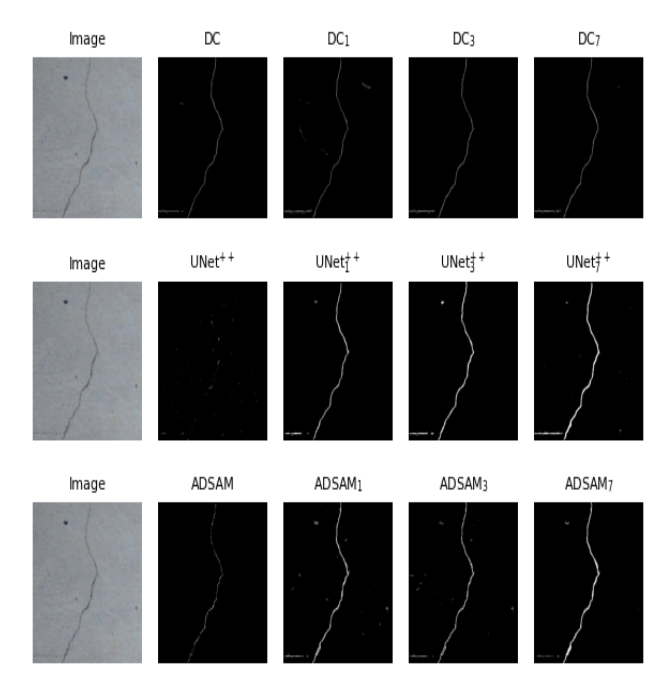


Figure 9: Shows original image, Model, Model₁, Model₃ and Model₇ outputs on EUGEN MULLER [18] dataset. The titles of each figure (except the crack images from the dataset) show the name of model used for inference.

improving an existing model with few images (improving generalization) and in turn, reducing the labelling and training cost while avoiding overfitting. We have shown that guiding the model with only a few images (see figure 7) from each of the secondary datasets can improve its performance significantly.

Our approach helps in explaining the behaviour of the models that can be seen in figures 2, 3, 4, 5, 6 and 9.

The proposed approaches can be extended to explain model behaviour on other deep learning tasks by selecting our distance metrics (see section 3.2) and a suitable performance metric (see section 3.3) for that task.

8. Acknowledgement

We would like to thank GE Research for providing us with the resources and a conducive environment that made this research possible.

References

- [1] Wang, Zhou, Alan C. Bovik, Hamid R. Sheikh, and Eero P. Simoncelli. "Image quality assessment: from error visibility to structural similarity." IEEE transactions on image processing 13.4 (2004): 600-612.
- [2] Dalal, Navneet, and Bill Triggs. "Histograms of oriented gradients for human detection." 2005 IEEE computer society conference on computer vision and pattern recognition (CVPR'05). Vol. 1. Ieee, 2005.
- [3] Koch, Gregory, Richard Zemel, and Ruslan Salakhutdinov. "Siamese neural networks for one-shot image recognition." ICML deep learning workshop. Vol. 2. No. 1. 2015.
- [4] Melekhov, Iaroslav, Juho Kannala, and Esa Rahtu. "Siamese network features for image matching." 2016 23rd international conference on pattern recognition (ICPR). IEEE, 2016.
- [5] Alvarez-Melis, David, and Nicolo Fusi. "Geometric dataset distances via optimal transport." Advances in Neural Information Processing Systems 33 (2020): 21428-21439.
- [6] Huai, Mengdi, et al. "Deep Metric Learning: The Generalization Analysis and an Adaptive Algorithm." IJ-CAI. 2019.
- [7] Cen, Jun, et al. "Deep metric learning for open world semantic segmentation." Proceedings of the IEEE/CVF International Conference on Computer Vision. 2021.
- [8] Rajagopal, Abhejit, et al. "Understanding and Visualizing Generalization in UNets." Medical Imaging with Deep Learning. PMLR, 2021.
- [9] Gevaert, Caroline M., and Mariana Belgiu. "Assessing the generalization capability of deep learning networks for aerial image classification using landscape metrics." International Journal of Applied Earth Observation and Geoinformation 114 (2022): 103054.
- [10] Petersen, E., Holm, S., Ganz, M., & Feragen, A. (2023). The path toward equal performance in medical machine learning. Patterns, 4(7).
- [11] Huang, W. R., Emam, Z., Goldblum, M., Fowl, L., Terry, J. K., Huang, F., and Goldstein, T. (2020). Understanding generalization through visualizations.
- [12] Kirillov, Alexander, et al. "Segment anything." arXiv preprint arXiv:2304.02643 (2023).
- [13] Chen, Tianrun, et al. "SAM Fails to Segment Anything?— SAM-Adapter: Adapting SAM in Underperformed Scenes: Camouflage, Shadow, and More." arXiv preprint arXiv:2304.09148 (2023).
- [14] Everingham, Mark, and John Winn. "The PASCAL visual object classes challenge 2012 (VOC2012) results. 2012
- [15] Arbelaez, Pablo, et al. "Contour detection and hierarchical image segmentation." IEEE transactions on pattern analysis and machine intelligence 33.5 (2010): 898-916.

- [16] Zou, Qin, Zheng Zhang, Qingquan Li, Xianbiao Qi, Qian Wang, and Song Wang. "Deepcrack: Learning hierarchical convolutional features for crack detection." IEEE Transactions on Image Processing 28.3 (2018): 1498-1512.
- [17] Eisenbach, Markus, Ronny Stricker, Daniel Seichter, Karl Amende, Klaus Debes, Maximilian Sesselmann, Dirk Ebersbach, Ulrike Stoeckert, and Horst-Michael Gross. "How to get pavement distress detection ready for deep learning? A systematic approach." In 2017 international joint conference on neural networks (IJCNN), pp. 2039-2047. IEEE, 2017.
- [18] 'Kaggle Crack Segmentation Dataset', https://www.kaggle.com/datasets/lakshaymiddha/cracksegmentation-dataset, accessed 2020
- [19] Lüddecke, Timo, and Alexander S. Ecker. "Prompt-based multi-modal image segmentation." arXiv preprint arXiv:2112.10003 (2021).
- [20] Tan, Mingxing, and Quoc Le. "Efficientnet: Rethinking model scaling for convolutional neural networks." International conference on machine learning. PMLR, 2019.
- [21] Deng, Jia, et al. "Imagenet: A large-scale hierarchical image database." 2009 IEEE conference on computer vision and pattern recognition. Ieee, 2009.
- [22] Zhou, Zongwei, et al. "Unet++: A nested u-net architecture for medical image segmentation." Deep Learning in Medical Image Analysis and Multimodal Learning for Clinical Decision Support: 4th International Workshop, DLMIA 2018, and 8th International Workshop, ML-CDS 2018, Held in Conjunction with MIC-CAI 2018, Granada, Spain, September 20, 2018, Proceedings 4. Springer International Publishing, 2018.
- [23] Radford, Alec, Jong Wook Kim, Chris Hallacy, Aditya Ramesh, Gabriel Goh, Sandhini Agarwal, Girish Sastry, Amanda Askell, Pamela Mishkin, Jack Clark, Gretchen Krueger, Ilya Sutskever. "Learning transferable visual models from natural language supervision." International conference on machine learning. PMLR, 2021.
- [24] He, Kaiming, et al. "Masked autoencoders are scalable vision learners." Proceedings of the IEEE/CVF conference on computer vision and pattern recognition. 2022.
- [25] Pedregosa, Fabian, et al. "Scikit-learn: Machine learning in Python." the Journal of machine Learning research 12 (2011): 2825-2830.
- [26] Iakubovskii, P. (2019). "Segmentation Models Pytorch." GitHub (2019).
- [27] Falcon, William A. "Pytorch lightning." GitHub 3 (2019).
- [28] Hunter, J. D. (2007). Matplotlib: A 2D graphics environment. Computing in science & engineering, 9(03), 90-95.
- [29] Pandey, Ram Krishna, and Akshit Achara. "TrueDeep: A systematic approach of crack detection with less data." arXiv preprint arXiv:2305.19088 (2023).

[30] Zhang, Renrui, et al. "Personalize segment anything model with one shot." arXiv preprint arXiv:2305.03048 (2023).

PC	S_1	S_2	S_3	S_4	S_5	S_6
5	0.078	0.097	0.087	0.073	0.453	0.214
10	0.068	0.084	0.077	0.065	0.486	0.220
15	0.063	0.077	0.071	0.061	0.491	0.237
20	0.057	0.071	0.064	0.055	0.466	0.287
25	0.056	0.069	0.063	0.054	0.465	0.293

Table 6

The table shows the values of $O^{dist}(S,P)$ computed by selecting varying number of prinicipal components(PC). The model used here is UNet⁺⁺ trained on P. Each value in the table is divided by the sum of its row.

A. Distances

A.1. Effect of the Number of Principal Components on Distances

The selection of the number of principal components can be divided into three cases.

- 1. **Case 1:** If the number of principal components selected for the distance computation is less than 15, it is observed that there is a significant difference in the distances with change in the number of principal components.
- 2. **Case 2:** If the number of principal components selected for the distance computation is between 15 and 25, there is very less difference in the distances with the change in number of principal components.
- 3. Case 3: If the number of principal components selected for the distance computation is greater than 25, there is negligible difference in the distances with the change in number of principal components.

The table 6 shows the decrease in difference of distances between the subsequent dimensions.

A.2. Distance Distributions

It can be seen in figure 10 that there is a steep increase in the distance of the images in the third split for S_4 for which there is a significant difference in the F-score of the first 33% and last 33% images. A consistent distribution can be seen for S_2 where all splits had similar F-scores. In general, the consistency and inconsistency in the distance distribution of the datasets is reflected in the performance (F-score). See table 3b for more details.

B. Are Cracks an Important Feature for Models?

B.1. SAM

The SAM can take points or boxes as prompts to produce output masks for input images. We give crack images as inputs to SAM along with prompt points and bounding boxes as shown in figure 11 and observe that the output masks are surfaces or the intricacies of the surface rather than cracks. It is also difficult to provide prompt points at exact crack pixels across multiple images using an automated process.

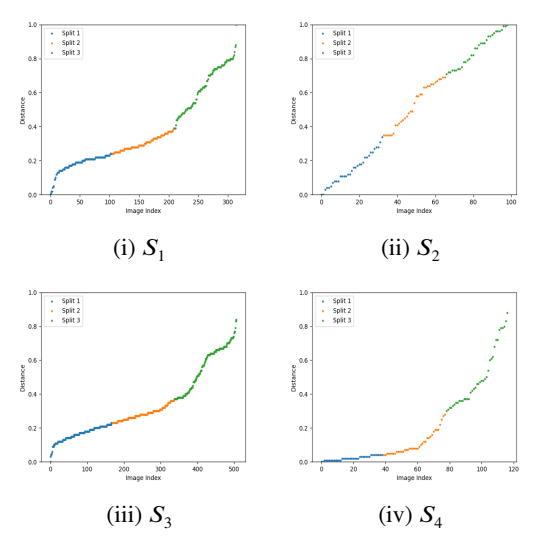
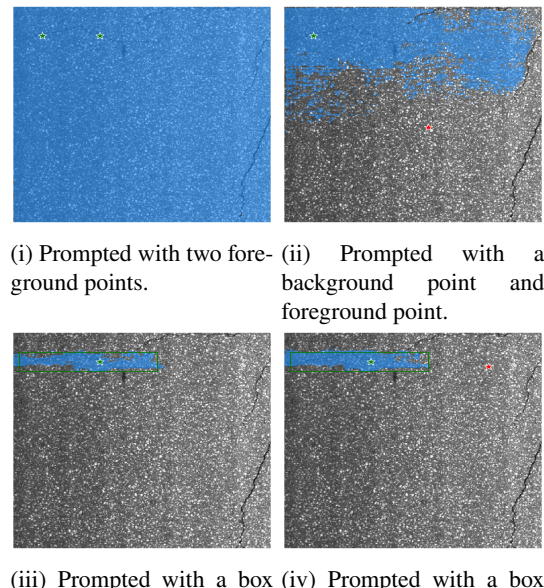


Figure 10: The figure shows the distribution of the distances of images in each secondary crack dataset S from the primary dataset P. The distances are computed using UNet⁺⁺ trained on P.



(iii) Prompted with a box (iv) Prompted with a box and foreground point in it. containing a foreground point and a background point outside the box.

Figure 11: The figure shows the predicted masks from the SAM model by inputting an image from S_1 . It can be observed that there is a focus on the surface (sometimes on the intricate details on the texture). However, cracks are not segmented here. Green points represent the foreground (crack) label prompt and red points represent the background label points.

It is to be noted that there was no tuning performed on SAM with crack data in this case. We have performed one-shot finetuning of SAM on P (see [30] for more details). There is no significant improvement in the crack detection. Finally, we have trained an adapted version of SAM (ADSAM [13])

to perform crack detection. ADSAM detects cracks from secondary crack datasets S similar to the other crack detection models.

B.2. CLIPSeg

We give multiple text prompts along with input crack images to the CLIPSeg model for zero-shot inference [19]. The output probability maps hightlight the crack regions but also capture background surfaces along the boundaries and other regions. Figure 12i shows the effect of input text prompts where the text prompt given for (a) is 'road pavement surface' and the model segments the surface whereas the prompts given for (b) and (c) are 'a crack or multiple cracks' and 'cracks on a road' where the model segments the crack regions. Figures 12ii and 12iii are not detecting the detecting the cracks at all or the boundaries are fuzzy. This suggests that the model needs to be trained for crack detection to perform similar to crack detection models. Finetuning of CLIPSeg requires labelled phrase region pairs that are not available for crack datasets.

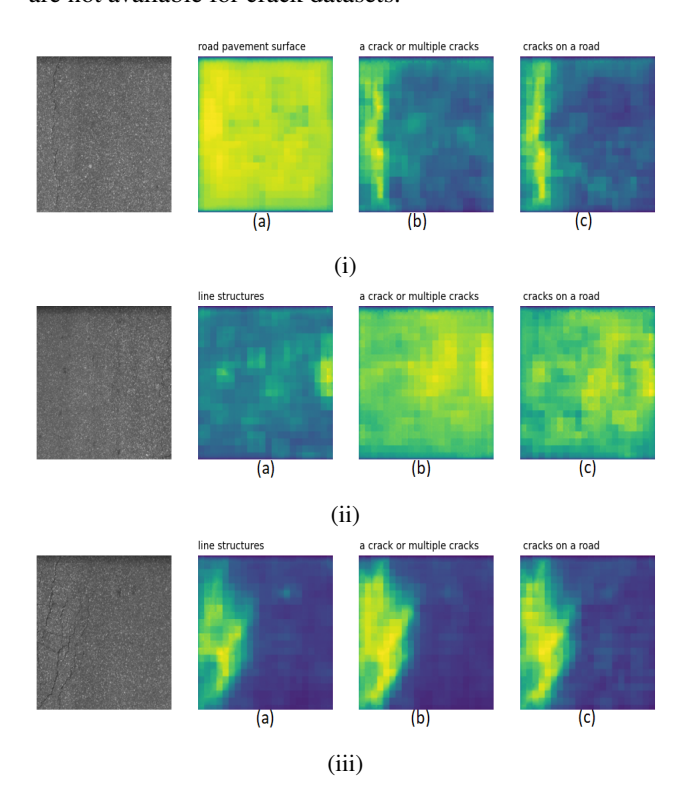


Figure 12: Shows (a) original image, (b) mask produced with prompt 1, (c) mask produced with prompt 2, (d) mask produced with prompt 3. The prompts can be seen in titles of the respective masks.